Phase-Shift Correction in Three-Dimensional Imaging Using Forward-Scattering Photoemission and Auger Spectroscopies

S. Y. Tong, C. M. Wei, T. C. Zhao, H. Huang, and Hua Li

Department of Physics and Laboratory for Surface Studies, University of Wisconsin–Milwaukee, Milwaukee, Wisconsin 53201

(Received 9 October 1990)

We invert high-energy ($E \geq 400$ eV) photoelectron and Auger-electron interference patterns to construct 3D images of surface and interface atoms. A new scheme is introduced to correct the phase shift of the image. Image reconstruction is demonstrated for Si(111)$\sqrt{3}\times\sqrt{3}$-B, a system in which multiple-scattering effects are small and all source waves are equivalent. Using diffraction results from multiple-scattering slab calculations, we achieve a spatial resolution of 1.0–1.3 Å, thus qualifying the technique as a direct structural tool.

PACS numbers: 68.35.Bs, 61.16.–d, 68.55.–a, 79.60.–i

The ability to construct three-dimensional atomic images from electron interference patterns has many exciting possibilities. Theoretical predictions and computer modeling play an important role in the development of this technique. Two types of scattering geometries are used: backward scattering of low- to moderate-energy electrons (100–500 eV),[1,2] and forward scattering of higher-energy electrons (400 to above 1000 eV).[3,4] In these studies, real-space imaging is obtained by two-dimensional Fourier transformation. The spatial resolution of the images formed in the plane normal to the surface is over 2 Å. Since the average distance between atoms in a solid is only $\simeq$2.5 Å, and the average interlayer spacing is less than 2 Å, to solve unknown structures a spatial resolution of $\simeq$1 Å is required for the technique to become practical.

A major source of error is the phase shift due to scattering of the electron by the atomic potentials. This phase shift causes images to be formed away from the atomic centers. The shift is in the range of 0.3–1.0 Å, and is present in both forward- and backward-scattering geometries. Multiple scattering and source waves emitted from different layers are other causes that degrade spatial resolution. In this paper, we present image reconstructions from forward-scattering photoelectron and Auger-electron diffraction patterns for a system in which multiple-scattering effects are small. In addition, the source waves are emitted from atoms in a single layer, making them equivalent. We also introduce a method that eliminates the phase error in the forward-scattering geometry. We show that with the use of a phase-corrected interference function, we achieve a practical resolution of $\simeq$1 Å.

The system studied here is Si(111)$\sqrt{3}\times\sqrt{3}R30°$-B (hereafter referred to as Si$\sqrt{3}$-B). This structure has been studied by scanning tunneling microscopy (STM),[5,6] x-ray diffraction,[7] photoemission,[8] and LEED,[9] and there is a general consensus on its atomic geometry. In this system, the B atoms occupy substitutional sites (i.e., the B_5 site) in the second layer (see Fig. 1). The atomic imaging is reconstructed from forward-scattering x-ray photoemission spectroscopy (XPS) patterns, at photoelectron energies 400–1000 eV. Photoelectrons at energies above 400 eV are strongly scattered in the forward direction by the core potentials of atoms. The intensity enhancement is the strongest along the emitter-scatterer direction (i.e., the focusing effect). In an angular cone surrounding each forward-focusing direction, the interference pattern is used to form three-dimensional images of atoms in the layer or layers *above* the emitter. Backward-scattering contributions to the scattering cone are 1–2 orders of magnitude smaller. Multiple scattering in the forward direction along a chain of atoms affect the interference patterns in the scattering cone, but in the case of Si$\sqrt{3}$-B these events do not exist since B is in the second layer.

The photoemission diffraction patterns are calculated for emission from the B 1*s* core level, at photoelectron energies 400 and 1000 eV. The photon incident direction and the electron exit angle are fixed at 70° apart while the crystal is rotated to generate the 2π hemispherical scan. The photon is *p* polarized. Although multiple scattering is expected to be small for the reasons stated

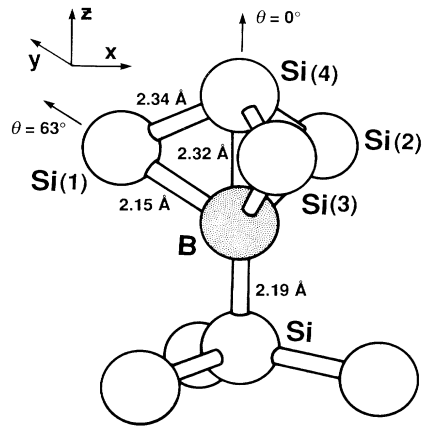

FIG. 1. Schematic diagram of Si(111)$\sqrt{3}\times\sqrt{3}R30°$-B surface geometry.

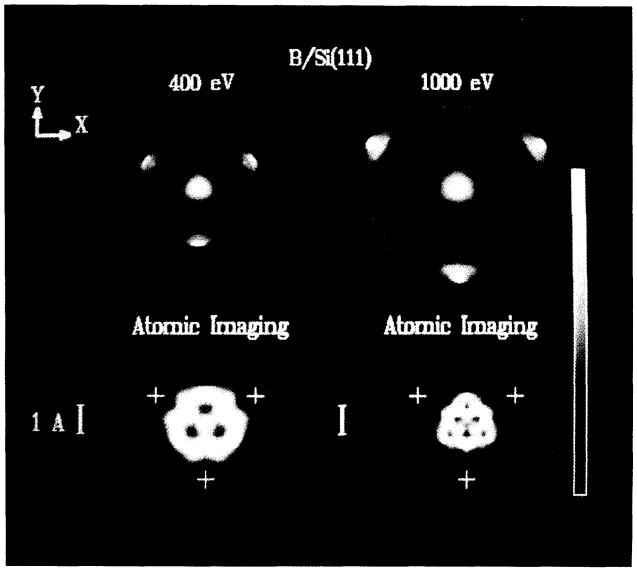

FIG. 2. Top panels: Hemispherical XPS intensity patterns in stereographical projection; radii equal $k_i=[(2m/\hbar^2)E_i]^{1/2}$. Lower panels: Atomic images of three Si atoms at $z=0.98$ Å cut above origin. The crosses indicate correct atomic centers. Color scale is shown on right.

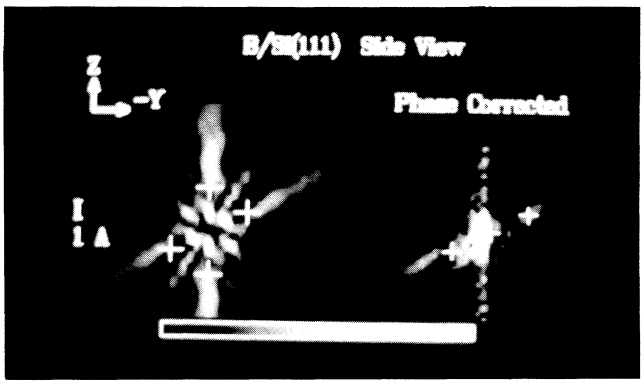

FIG. 3. Side view at $x=0$ cut. Left: Images and twins for Si(3) and Si(4) atoms with no phase correction. Right: Phase-corrected image of Si(3) at cross in ($z\geq 0$, $y\leq 0$) quadrant (i.e., at 2 o'clock direction).

above, nevertheless, the simulations are based on the multiple-scattering slab method, which includes all orders of forward- and backward-scattering events.[10] The three-dimensional surface structure determined by LEED is used in the simulation.[9] In Fig. 2, we show the hemispherical diffraction patterns for 400 and 1000 eV (upper left and right), respectively. The most striking features are the four focusing spots, which have a one-to-one correspondence to the B-Si internuclear directions, at polar angles $\theta=0°$ and 63°. The lack of energy dependence of the focusing peak is a theoretical prediction based on quantum-mechanical diffraction concepts[11-13] and confirmed by experiments.[14-18]

The 2π-sr diffraction patterns are inverted to produce three-dimensional real-space images $\phi(x,y,z)$ which may be viewed in different planar sections.[1-4] Figure 2 lower left and right panels show the images from transforming the 400- and 1000-eV 2π scans, respectively, at a cut parallel to the surface, at height $z=0.98$ Å *above* the B atom. This cut passes through the nuclei of the three nearest-neighbor Si atoms (1, 2, and 3) of Fig. 1. The crosses mark the actual Si nuclei positions. The true test of spatial resolution, however, is not in planar views at known z cuts. The forward-focusing peaks provide the symmetry of the system from which we cut along the y-z plane to pass through the nuclei of Si atoms 3,4 and the B atom. In the forward-scattering geometry, the scattering factor decays rapidly as $\theta_{\hat{\mathbf{k}}}$, the scattering angle measured from the emitter-scatter direction, increases. This limits the range of $\Delta\mathbf{k}_\parallel$ and Δk_z in the transform. The limitation is especially severe for $k_z=k_0(1-\cos\theta_{\hat{\mathbf{k}}_\parallel})$, where $k=[(2m/\hbar^2)E]^{1/2}$ is the photoelectron's wave vector. Since $\Delta z\propto 1/\Delta k_z$, the image in the y-z plane is elongated and points towards the origin (i.e., the B atom). In Fig. 3 (left panel), we show the y-z planar view of atomic images reconstructed from the 400-eV diffraction pattern. The images of Si atoms 3 and 4 are seen (in the $y\leq 0$, $z\geq 0$ quadrant), together with their twin images (in the $y\geq 0$, $z\leq 0$ quadrant). Again, the crosses mark the correct atomic centers. There is substantial error in the image position ($\simeq$0.5–1.0 Å) and the resolution is poor. *Three-dimensional images of this quality provide little quantitative information about surface structure.*

To make this technique quantitative and practical, we need to understand the origin of the errors. To construct atomic images, we transform an interference enhancement function $\chi(\hat{\mathbf{k}})=[I(\hat{\mathbf{k}})-A]/A$, where $I(\hat{\mathbf{k}})$ is the measured or calculated diffraction intensity and A is its angle-averaged value. In the forward-scattering geometry, $\chi(\hat{\mathbf{k}})$ is made up of local regions each dominated by forward scattering by a particular atom or chain of atoms. Thus, using the small-atom approximation,[19] we can write $\chi(\hat{\mathbf{k}})$ as[20]

$$\chi(\hat{\mathbf{k}})\propto\sum_i\frac{|F_D(\hat{\mathbf{R}}_i)|^2|f(\theta_i)|^2}{|F_D(\hat{\mathbf{k}})|^2R_i^2}+\sum_i\frac{F_D(\hat{\mathbf{R}}_i)f(\theta_i)e^{ikR_i(1-\cos\theta_i)}}{F_D(\hat{\mathbf{k}})R_i}+\text{c.c.}+\cdots, \tag{1}$$

where $\hat{\mathbf{R}}_i$ are emitter-scatterer internuclear vectors, $f(\theta_i)\equiv f((\mathbf{k}-\mathbf{R}_i)/|\mathbf{k}-\mathbf{R}_i|)$ are scattering form factors whose angle is measured from each internuclear direction $\hat{\mathbf{R}}_i$, and $F_D(\hat{\mathbf{k}})$ is the XPS source wave at the emitter.[12,19] The first

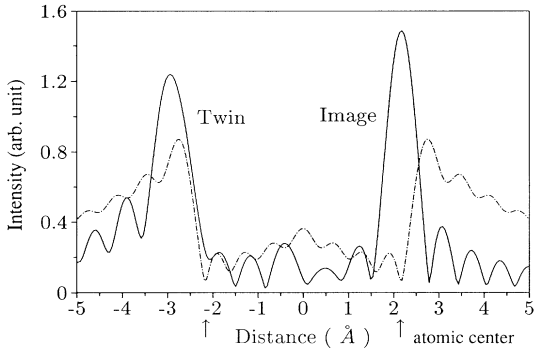

FIG. 4. Transformed functions of $\chi(\theta)$ (dot-dashed line) and $g(\theta)$ (solid line). The emitter is at the origin, the positions of the scatterer and its twin are indicated by arrows.

term in Eq. (1) is the square of the object waves and the atomic images are formed from the second term.[20] The complex-conjugate term produces the twin images. Higher-order terms contain multiple-scattering and mixed-$\hat{\mathbf{R}}_i$-$\hat{\mathbf{R}}_j$ contributions.

The phase shift comes from the complex scattering factor $f(\theta_i)=|f(\theta_i)|\exp(i\psi_{\theta_i})$. We illustrate this effect by a two-atom system, in which an emitter is placed at the origin and a scatterer at $z=2.15$ Å. To further simplify the illustration, we set $F_D(\hat{\mathbf{R}})=F_D(\hat{\mathbf{k}})$, i.e., we simulate an isotropic source wave as in the case of a high-energy Auger electron. We keep the kinetic energy at 400 eV and calculate $\chi(\theta)$, θ measured from the z axis, for the two-atom case. To eliminate the shift caused by ψ_θ we construct a new function $g(\theta)=\chi(\theta)/f(\theta)$. We note that $g(\theta)$ is complex and the division by $f(\theta)$ achieves two results: (i) The unwanted phase ψ_θ is eliminated and (ii) $g(\theta)$ no longer has a rapidly decaying envelope, and, thus, the range of usable k is extended.

The effect of this phase correction is very evident from the transformed functions shown in Fig. 4. The transform of $\chi(\theta)$ (dot-dashed line), which is not phase corrected, has a peak shifted by $\sim$0.62 Å from the correct atomic position (indicated by an arrow). This function has a multipeak shoulder (i.e., streaky image) at higher z values. On the other hand, the transform of the phase-corrected function $g(\theta)$ (solid line) peaks at the correct atomic position. This peak is more intense and the shoulder is absent (i.e., improved resolution). Another advantage is that its twin image is shifted further away from the correct atomic position, because the forward-scattering phase of the complex-conjugate term in Eq. (1) has the opposite sign. Thus, the phase correction breaks the symmetry of the real image and its twin, and the latter may be discarded. The division by $f(\theta_i)$ has two components: (i) Division by $|f(\theta_i)|$ removes the strong anisotropy in $\chi(\theta_i)$ and, in this case, shifts the image (and its twin) by $\sim$0.22 Å towards the correct position; (ii) division by $\exp(i\psi_{\theta_i})$ shifts the image by $\sim$0.40 Å towards the correct atomic center while shifting the twin image by $\sim$0.80 Å away from the corresponding twin atomic center.[21]

We apply these ideas to the exact (i.e., small-atom and isotropic-source-wave approximations not used) interference function $\chi(\hat{\mathbf{k}})$ (Ref. 15) calculated for the Si$\sqrt{3}$-B system. This system has multiple focusing directions; hence the phase correction is done separately for each atom. For example, to phase correct the image of Si atom 3, we divide $\chi(\hat{\mathbf{k}})$ by a correction function of the following form:

$$p_3(\hat{\mathbf{k}})=\frac{f(\theta_3)}{|f(\theta_3)|}\sum_j|f(\theta_j)|\,, \tag{2}$$

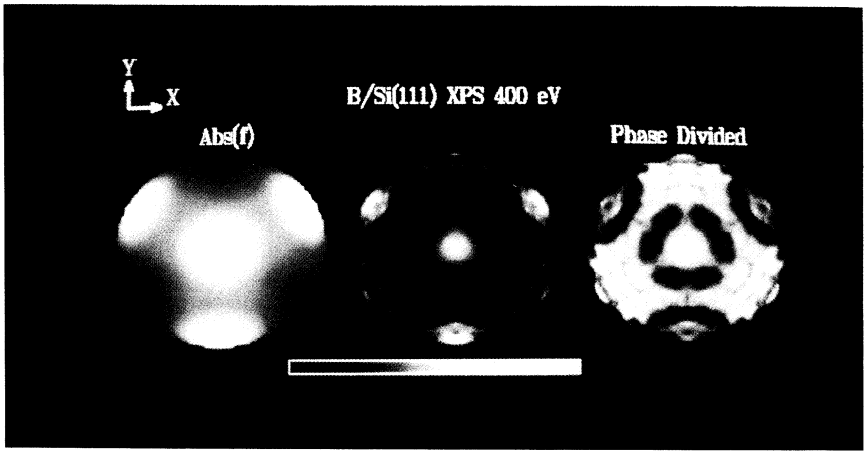

FIG. 5. Left: Absolute value of the correction function. Center: XPS intensity pattern as in Fig. 1. Right: Absolute value of the phase-corrected function shown in stereographical projection.

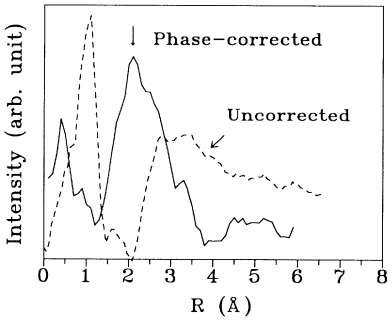

FIG. 6. Intensity variation of phase-corrected and uncorrected images along the B-Si(3) internuclear direction; the origin is at the B-atomic center.

where θ_3 is the scattering angle relative to $\hat{\mathbf{R}}_3$, the focusing direction determined from the $\hat{\mathbf{k}}$-space diffraction pattern for Si atom 3, and j runs over the four focusing directions. In Fig. 5, we show the absolute value of the correction function $p_3(\hat{\mathbf{k}})$ (left panel), the original function $\chi(\hat{\mathbf{k}})$ (middle panel), and the absolute value of the phase-corrected function $g(\hat{\mathbf{k}})=I(\hat{\mathbf{k}})/p_3(\hat{\mathbf{k}})$ (right panel). The Fourier transform of $g(\hat{\mathbf{k}})$ is shown in Fig. 3, right panel, where the only physically meaningful real-space image is that of Si(3) (in the $y\leq 0$, $z\geq 0$ quadrant). We mark the origin (i.e., center of the B atom), the correct Si atom 3 position, and its inversion vector by three crosses. Figure 6 shows the intensity variation of the image along the B-Si(3) internuclear direction. For the phase-corrected curve (solid line), the intensity peaks at 2.11 Å compared to the correct value of 2.15 Å, an error of only 0.04 Å. The full width at half maximum is 1.3 Å. The phase correction is applied in turn to each focusing direction. After discarding the unphysical images, a composite three-dimensional image of the surface structure is obtained. Of course, it is not necessary to reconstruct more than once the images of Si atoms that are related by symmetry. In Eq. (2), the sum over j does not have to include all the focusing directions, especially if some directions are very close together. However, for best results (i.e., noise reduction), one should include complete sets of focusing directions that are related by symmetry.

In summary, we have introduced the use of a phase-correction procedure which enables forward-scattering XPS–Auger-electron spectroscopy holography to achieve a practical resolution of $\simeq 1.0$ Å. This qualifies the technique as a direct structural tool. Forward-scattering holography (FSH), with the phase correction, images actual atomic core centers where the forward scattering is strongest. FSH is species specific and it provides coordination information of at least two layers of atoms; thus it is better suited for studying the heterogeneous interface. Theoretical modeling and computation simulations, to test the limits of new or improved image reconstruction, will remain central to the development of this technique.

This work is supported in part by ONR Grant No. N00014-90-J-1749.

[1]J. J. Barton, Phys. Rev. Lett. **61**, 1345 (1988).
[2]D. K. Saldin and P. L. de Andres, Phys. Rev. Lett. **64**, 1270 (1990).
[3]G. R. Harp, D. K. Saldin, and B. P. Tonner, Phys. Rev. Lett. **65**, 1012 (1990).
[4]C. M. Wei, T. C. Zhao, and S. Y. Tong, Phys. Rev. Lett. **65**, 2278 (1990).
[5]P. Bedrossian, R. D. Meade, K. Mortensen, D. M. Chen, J. A. Golovchenko, and D. Vanderbilt, Phys. Rev. Lett. **63**, 2357 (1989).
[6]I.-W. Lyo, E. Kaxiras, and Ph. Avouris, Phys. Rev. Lett. **63**, 1261 (1989).
[7]L. Headrick, I. K. Robinson, E. Vlieg, and L. G. Feldman, Phys. Rev. Lett. **63**, 1253 (1989).
[8]E. Kaxiras, K. C. Pandey, F. J. Himpsel, and R. M. Tromp, Phys. Rev. B **41**, 1262 (1990).
[9]H. Huang, S. Y. Tong, J. Quinn, and F. Jona, Phys. Rev. B **41**, 3276 (1990).
[10]C. H. Li, A. R. Lubinsky, and S. Y. Tong, Phys. Rev. B **17**, 3128 (1978).
[11]H. C. Poon and S. Y. Tong, Phys. Rev. B **30**, 6211 (1984).
[12]S. Y. Tong, H. C. Poon, and D. R. Snider, Phys. Rev. B **32**, 2096 (1985).
[13]M. L. Xu and M. A. Von Hove, Surf. Sci. **207**, 215 (1989).
[14]S. A. Chambers, S. B. Anderson, and J. H. Weaver, Phys. Rev. B **32**, 4872 (1985).
[15]W. F. Egelhoff, Jr., Crit. Rev. Solid State Mater. Sci. **16**, 213 (1990).
[16]C. S. Fadley, in *Synchrotron Radiation Research; Advances in Surface Science,* edited by R. Z. Bachrach (Plenum, New York, 1989).
[17]H. Li and B. P. Tonner, Phys. Rev. B **37**, 3959 (1988).
[18]X. D. Wang, Z. L. Han, B. P. Tonner, Y. Chen, and S. Y. Tong, Science **248**, 1129 (1990).
[19]H. C. Poon, D. R. Snider, and S. Y. Tong, Phys. Rev. B **33**, 2198 (1986).
[20]C. M. Wei, T. C. Zhao, and S. Y. Tong, Phys. Rev. B (to be published).
[21]Hua Li and S. Y. Tong, Phys. Rev. B (to be published).

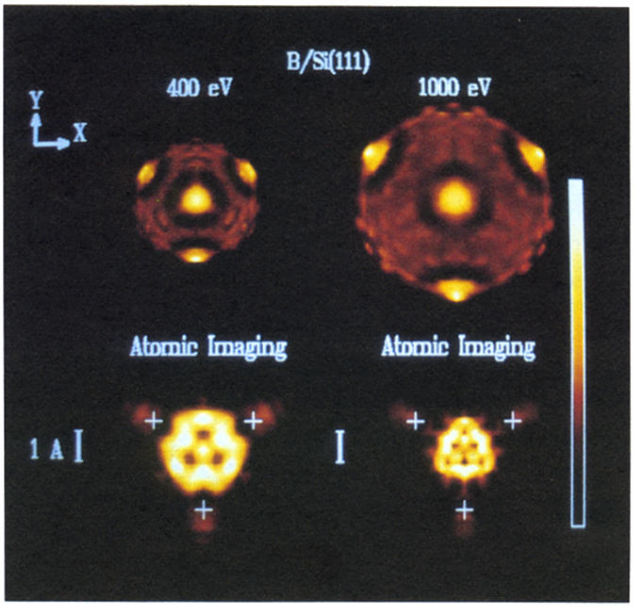

FIG. 2. Top panels: Hemispherical XPS intensity patterns in stereographical projection; radii equal $k_i = [(2m/\hbar^2)E_i]^{1/2}$. Lower panels: Atomic images of three Si atoms at $z = 0.98$ Å cut above origin. The crosses indicate correct atomic centers. Color scale is shown on right.

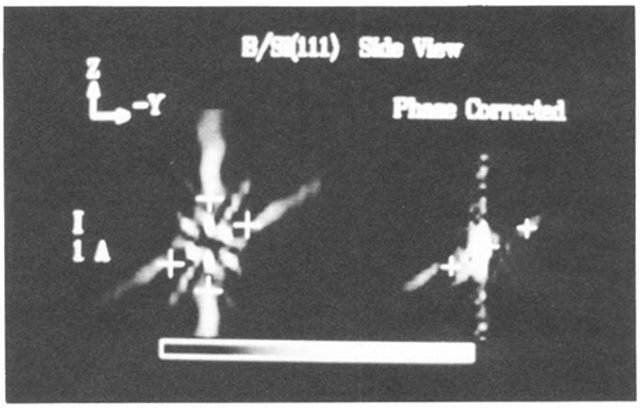

FIG. 3. Side view at $x=0$ cut. Left: Images and twins for Si(3) and Si(4) atoms with no phase correction. Right: Phase-corrected image of Si(3) at cross in ($z \geq 0$, $y \leq 0$) quadrant (i.e., at 2 o'clock direction).

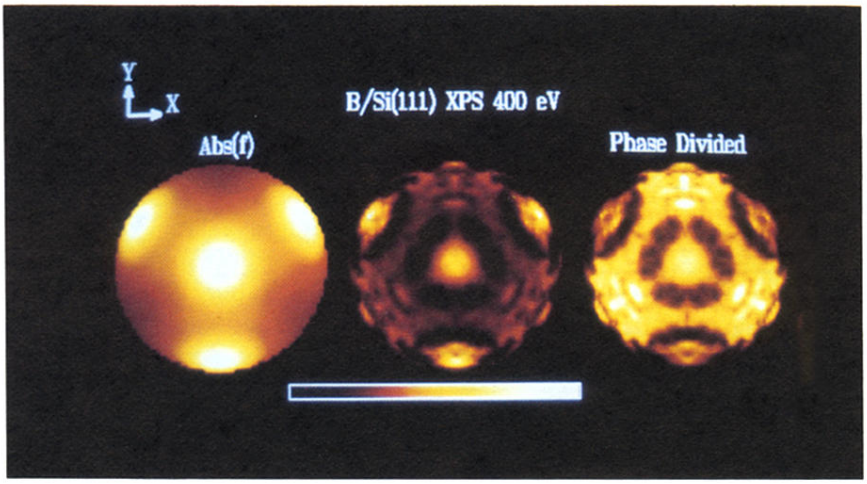

FIG. 5. Left: Absolute value of the correction function. Center: XPS intensity pattern as in Fig. 1. Right: Absolute value of the phase-corrected function shown in stereographical projection.